A Model for the Interpretation of the Absorption and Circular Dichroism Spectra of Tris(di-imine) Complexes of Iron(II) and Ruthenium(II)

Claude Daul and Carl Wilhelm Schlaepfer
Institut de Chimie Inorganique et Analytique, Universite de Fribourg, Perolles, CH-1700 Fribourg, Switzerland

A theoretical model of the electronic structure of the metal-to-ligand charge-transfer (m.l.c.t.), ligand-centred (l.c.) and metal-centred (m.c.) states of tris(di-imine)metal(II), $[ML_3]^{2+}$ (M = Fe or Ru), is developed. The model contains only three adjustable parameters describing the first-order mixing of metal and ligand wavefunctions. All the state matrix elements are simplified by tensor operator techniques to reduced one-electron matrix elements, which are calculated numerically using Slater type orbitals. A quantitative prediction of the absorption and circular dichroism spectra, including all spin-allowed m.l.c.t., l.c., and m.c. bands of $[ML_3]^{2+}$ is made, using a reasonable set of mixing parameters, which is in good agreement with the experimental results.

There is a great interest to know the electronic structure of d^6 tris(α-di-imine) complexes in order to gain more detailed insight to their photophysical properties. A very stringent test for any model is the simultaneous explanation of the main features of the absorption and the circular dichroism (c.d.) spectra. The models proposed so far[1-5] have only been successful in the interpretation of the metal-to-ligand charge-transfer (m.l.c.t.) and ligand-centred bands (l.c.) of the absorption spectrum and the l.c. bands of the c.d. spectrum.[6] A satisfactory description of the c.d. bands due to m.l.c.t. and metal-centred (m.c.) transitions is still lacking to our knowledge. The main reasons are as follows. (i) Recently Ferguson *et al.*[7] published single-crystal c.d. spectra of these complexes, which allow an unambiguous assignment of the c.d. transitions. (ii) In order to calculate the rotational strength, both the electric and magnetic transition moments have to be known. These moments can be very different in origin and magnitude as exhibited by the m.l.c.t. transitions (see below). Hence the model has to include both mechanisms, one leading to electric dipole moments and one leading to large magnetic moments. (iii) There is no general agreement whether the calculation of rotational strength based on approximate wavefunctions should be based on the dipole velocity or the dipole length operator. Dipole velocity is known to guarantee origin-independent rotational strength, whereas experience shows that dipole length is in general successfully applied for the estimation of absolute values of electric dipole moments even from very crude wavefunctions.[8] As we show in the Appendix, rotational power calculations based on electric dipole lengths are origin-independent also, provided that the symmetry of the system is sufficiently high so that the three directions of a cartesian co-ordinate system span different components of different irreducible representations. This is the case for tris(α-di-imine) complexes. Hence there is no reason not to use the dipole length formalism for both calculations: the line and rotational strengths.

Theoretical Model

Calculation of Line and Rotational Strengths.—The line strength of an optical transition is determined by its electrical transition dipole moment, equation (1), where $\langle A|$ and $|B\rangle$

$$\text{Line strength} \sim |\langle A|\Sigma\vec{r}_i|B\rangle|^2 \qquad (1)$$

are the determinantal wavefunctions of the ground and excited states respectively and $\vec{r}_i$ the co-ordinates of the ith electron. The c.d. intensities, *i.e.* the rotational strengths, are determined by the imaginary part of the scalar product of the electrical and magnetic transition dipole moments, equation (2), where the

$$\text{Rotational strength, } R \sim \langle A|\Sigma\vec{r}_i|B\rangle\cdot\langle B|\vec{r}_i \times \vec{\nabla}_i|A\rangle \qquad (2)$$

symbols used are the same as above and $\vec{\nabla}_i$ is the gradient operator acting on the co-ordinates of the ith electron. Using irreducible tensor operators[8] these state matrix elements are easily related to one-electron matrix elements, equation (3).

$$\langle a^n\,{}^1A_1\|U^f\|a^{n-1}(\tfrac{1}{2}a)\,b(\tfrac{1}{2}b)^1\Gamma\rangle = 2\cdot\dim(\Gamma)\cdot\dim(b)\cdot W\begin{Bmatrix} a & b & f \\ A_1 & \Gamma & b \end{Bmatrix}\cdot\langle a\|u^f\|b\rangle \qquad (3)$$

The left-hand side of equation (3) represents a reduced state matrix element of an operator U spanning the irreducible representation f of the point group D_3 between the closed shell $\langle a^n\,{}^1A_1|$ (ground state) and the singly excited singlet $|a^{n-1}(\frac{1}{2}a)\,b(\frac{1}{2}b)\,{}^1\Gamma\rangle$ (excited state). This reduced state matrix element is related to a one-electron reduced matrix element between the donor orbital of symmetry a and the acceptor orbital of symmetry b multiplied by a W-coefficient, given in ref. 9, and a factor including the dimensions of the irreducible representations Γ and b. The symbols used in equation (3) are those introduced by Griffith.[9] The calculation of the reduced matrix elements is given by the Wigner–Eckart theorem, equation (4),

$$\langle a\alpha|u^f_\varphi|b\beta\rangle = \langle a\|u^f\|b\rangle\cdot V\begin{Bmatrix} a & b & f \\ \alpha & \beta & \varphi \end{Bmatrix} \qquad (4)$$

where a, b, and f are an irreducible representation of D_3; α, β, and φ are their components. The symbol on the right-hand side of equation (4) is a V-coefficient, given in ref. 9.

Molecular Orbital Diagram and Basis Functions.—Molecular orbital (m.o.) calculations (EHMO, MSXα, INDO, *etc.*) of $[ML_3]^{2+}$ (L = di-imine) have shown that the electronic transitions in the u.v.–visible region are due to transitions from the occupied orbitals to the unoccupied orbitals in the m.o. diagram in Figure 1.[3,10] Three types of transitions are possible: (i) metal-to-ligand charge transfer (m.l.c.t.), *i.e.* $t_{2_g}\rightarrow\pi^*$; (ii) metal-centred (m.c.) or ligand-field transitions, $t_{2_g}\rightarrow e_g$; (iii) ligand-centred (l.c.), $\pi\rightarrow\pi^*$; Rydberg transitions, *e.g.* $nd\rightarrow(n+1)p$ and $n\rightarrow\pi^*$, have been omitted. They were included in a preliminary analysis but their contribution was found to be negligible.

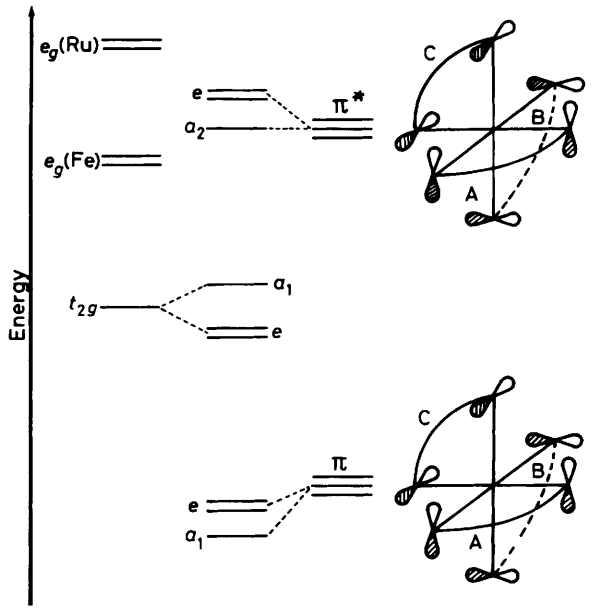

Figure 1. Molecular orbital diagram of $[M(bipy)_3]^{2+}$ (bipy = 2,2'-bipyridyl)

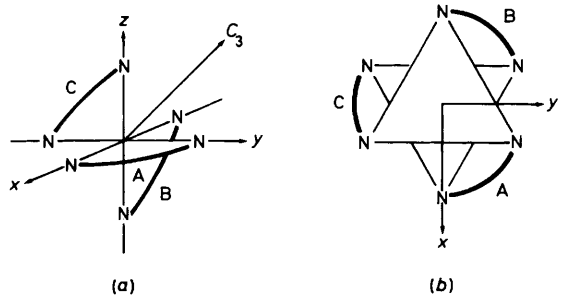

Figure 2. Co-ordinate systems of $[M(bipy)_3]^{2+}$: (*a*) $\{-1,1,1\}$ direction is C_3 axis, (*b*) *z* axis is C_3 axis. The transformation (*a*) ⟶ (*b*) is obtained through the following rotation:

$$\vec{r}_b = \begin{bmatrix} 1/\sqrt{6} & -1/\sqrt{6} & 2/\sqrt{6} \\ 1/\sqrt{2} & 1/\sqrt{2} & 0 \\ -1/\sqrt{3} & 1/\sqrt{3} & 1/\sqrt{3} \end{bmatrix} \cdot \vec{r}_a$$

The $[ML_3]^{2+}$ moiety has exact D_3 symmetry [11] (see Figure 2). Nevertheless a gross examination of the electronic structure reveals a close resemblance to octahedral symmetry, the trigonal splitting being small. In this latter symmetry, the metal t_{2g} orbitals transform as a_1 and e. The three π^* ligand orbitals (below) span a basis for an a_2 and e representation. The three π

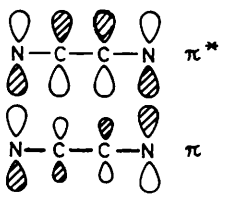

ligand orbitals span a basis for a_1 and e representation. Since only orbitals with the same symmetry label can interact, the following m.o. combinations are obtained: empty orbitals [equations (5a)]; occupied orbitals [equations (5b)]. The labels

Table 1. Symmetry-adapted basis functions using the co-ordinates of Figure 2(*a*)†

$$\begin{aligned}
|d\sigma\,\varepsilon\rangle &= -d_{x^2-y^2} \\
|d\sigma\,\theta\rangle &= d_{z^2} \\
|d\pi\,a_1\rangle &= (-d_{xy} - d_{xz} + d_{yz})/\sqrt{3} \\
|d\pi\,\theta\rangle &= (2d_{xy} - d_{xz} + d_{yz})/\sqrt{6} \\
|d\pi\,\varepsilon\rangle &= (d_{xz} + d_{yz})/\sqrt{2} \\
|\pi\,a_1\rangle &= (\chi_A + \chi_B + \chi_C)/\sqrt{3} \\
|\pi\,\theta\rangle &= (2\chi_A - \chi_B - \chi_C)/\sqrt{6} \\
|\pi\,\varepsilon\rangle &= (\chi_B - \chi_C)/\sqrt{2} \\
|\pi^*\,a_2\rangle &= (\psi_A + \psi_B + \psi_C)/\sqrt{3} \\
|\pi^*\,\varepsilon\rangle &= (2\psi_A - \psi_B - \psi_C)/\sqrt{6} \\
|\pi^*\,\theta\rangle &= (\psi_B - \psi_C)/\sqrt{2}
\end{aligned}$$

† θ and ε denote the two components of the representation *e*, as obtained from an extended Hückel calculation of NH=CH–CH=NH using standard calculation parameters (Quantum Chemistry Program Exchange, no. 344).

$$\chi = -0.6295\,p_z(N) + 0.6295\,p_z(N') - 0.2434\,p_z(C) + 0.2434\,p_z(C')$$

$$\psi = -0.5347\,p_z(N) - 0.5347\,p_z(N') + 0.5337\,p_z(C) + 0.5337\,p_z(C')$$

$$\begin{aligned}
e(e_g) &= |d\sigma\rangle + a\cdot|\pi^*\rangle \\
e(\pi^*) &= |\pi^*\rangle - b\cdot|d\pi\rangle \\
a_2(\pi^*) &= |\pi^*\rangle
\end{aligned} \qquad (5a)$$

$$\begin{aligned}
a_1(t_{2g}) &= |d\pi\rangle + c\cdot|\pi\rangle \\
e(t_{2g}) &= |d\pi\rangle + d\cdot|\pi\rangle + e\cdot|\pi^*\rangle \\
e(\pi) &= |\pi\rangle + f\cdot|d\pi\rangle \\
a_1(\pi) &= |\pi\rangle - g\cdot|d\pi\rangle
\end{aligned} \qquad (5b)$$

in parentheses denote the dominant character of the m.o.s. The functions in $|\rangle$ are obtained by symmetry-adapted linear combination (s.a.l.c.) of atomic orbitals (a.o.s). They are defined in Table 1. The coefficients *a*, *b*, *c*, *d*, *e*, *f*, *g* are small mixing coefficients with $b = e$, $c = 2d$, $g = c$, and $f = d$ if first-order perturbation is used. Thus in our model only three independent parameters remain (*a*, *b*, and *c*) which can be adjusted by trial and error.

Numerical Evaluation of the Orbital Transition Moments.— The calculation of these elements is lengthy and tedious. Thus we developed a computer program for their evaluation. The calculation flow chart is shown in the Scheme, where *N* is the number of a.o.s φ_μ in a s.a.l.c. $\psi_i = \Sigma c_{\mu i}\varphi_\mu$, $\vec{r}_A$ are the co-ordinates of the electron centred on atom A, and $\vec{r}_B$ the co-ordinates of the same electron but centred on atom B; $\vec{R}_A$ and $\vec{R}_B$ are the co-ordinates of atoms A and B respectively; $\vec{D}_{\mu\nu}$ and $\vec{D}_{ij}$ are the matrix elements of the electrical transition dipole moment in the a.o. and s.a.l.c. basis respectively; $\vec{M}_{\mu\nu}$ and $\vec{M}_{ij}$ are the matrix elements of the magnetic transition dipole moment in the a.o. and s.a.l.c. basis respectively. The a.o.s $\varphi_\mu(\vec{r})$ used in boxes 1 and 2 of the Scheme are Slater type orbitals, defined as in equation (6).

$$\varphi(\vec{r}) = |n,l,m,\zeta\rangle \qquad (6)$$

For the calculation of the integrals in boxes 1 and 2 (Scheme) the following relations have been used.

Electrical dipole matrix elements. These were obtained using equation (7), leading to the one-centre integrals in equation (8),

$$\vec{r} = \begin{bmatrix} x \\ y \\ z \end{bmatrix} = (4\pi/3)^{\frac{1}{2}}\cdot r\cdot \begin{bmatrix} Y_{l1}(\theta,\varphi) \\ Y_{l-1}(\theta,\varphi) \\ Y_{l0}(\theta,\varphi) \end{bmatrix} = \begin{bmatrix} q_1 \\ q_{-1} \\ q_0 \end{bmatrix} \qquad (7)$$

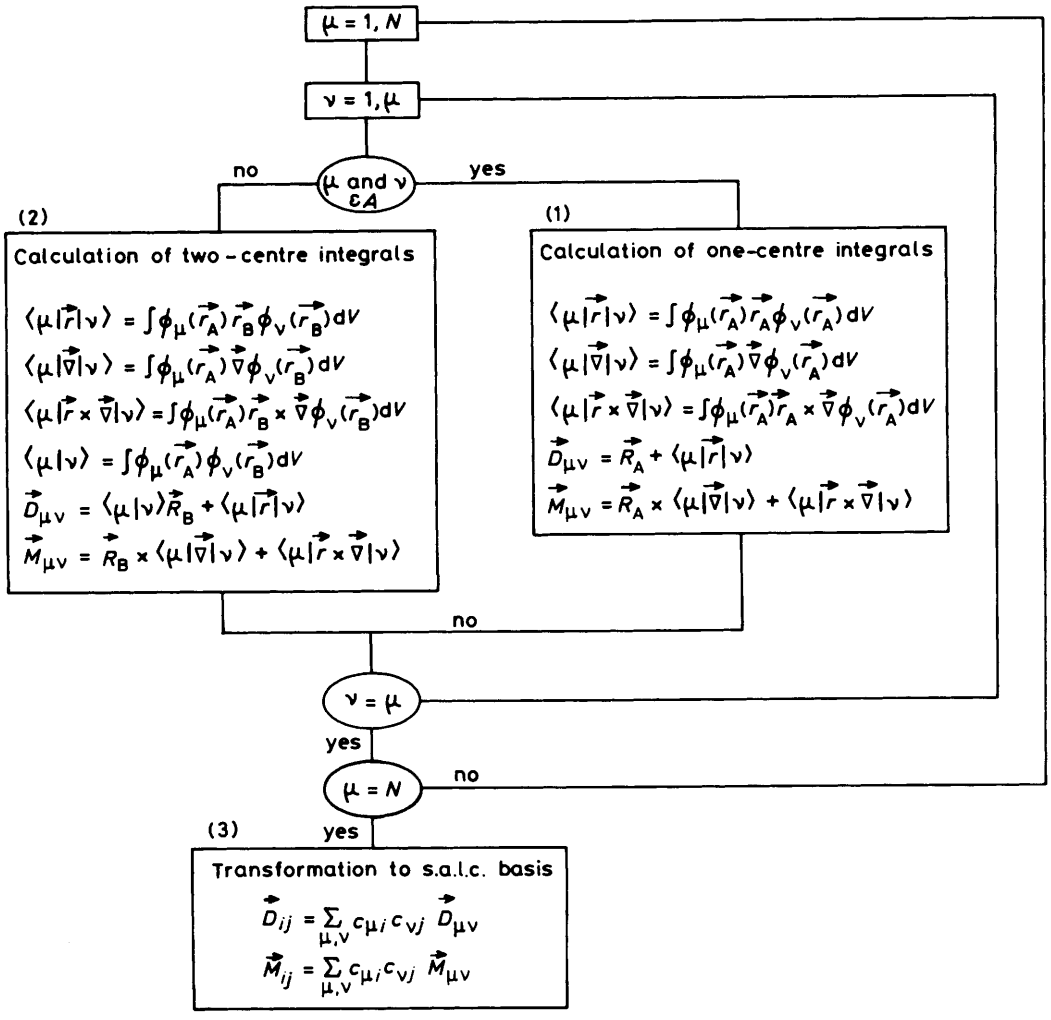

Scheme.

$$\langle nlm\zeta|q_\mu|n'l'm'\zeta'\rangle = (4\pi/3)^{\frac{1}{2}}\cdot[(n+n'+1)/(\zeta+\zeta')]\cdot C^{m\mu m'}_{l\,1\,l'}\cdot\langle nlm\zeta|n'l'm'\zeta'\rangle \quad (8)$$

$$C^{mm'M}_{l\,l'\,L} = \int Y_{lm}(\Omega)\cdot Y_{l'm'}(\Omega)\cdot Y_{LM}(\Omega)\cdot d\Omega \quad (9)$$

where equation (9) applies and $\langle nlm\zeta|n'l'm'\zeta'\rangle$ is the overlap integral between the two Slater type orbitals. The calculation of overlap integrals and C-coefficients is a standard quantum mechanical procedure and a detailed description of their evaluation is omitted here. For the two-centre integrals we have equation (10), where A and B represent the atoms on which the integration co-ordinates are centred.

Gradient matrix elements. If $\nabla_\mu = (\partial/\partial x, \partial/\partial y, \partial/\partial z)$ with $\mu = 1, -1, 0$ respectively we obtain equation (11) for the non-vanishing one-centre integrals, and equation (12) for the two-centre integrals, where all the symbols are consistent with those above.

Angular momentum matrix elements. The angular momentum operator $\vec{l} = \vec{r} \times \vec{\nabla}$ acts only on the angular part of the wavefunction. The calculation of its matrix elements is well known.

$$\langle n_A l_A m_A \zeta_A|q_\mu|n_B l_B m_B \zeta_B\rangle = [4\pi(n_B+1)\cdot(n_B+\tfrac{1}{2})/3]^{\frac{1}{2}}/\zeta_B\cdot\left[\sum_M C^{M}_{l_B+1\,1\,l_B}{}^{\mu m_B}\cdot\langle n_A l_A m_A\zeta_A|n_B+1,l_B+1,M,\zeta_B\rangle + \sum_M C^{M}_{l_B-1\,1\,l_B}{}^{\mu m_B}\cdot\langle n_A l_A m_A\zeta_A|n_B+1,l_B-1,M,\zeta_B\rangle\right] \quad (10)$$

$$\langle nl'\pm 1m\zeta|\nabla_\mu|n'l'm'\zeta'\rangle = (4\pi/3)^{\frac{1}{2}}\cdot[(n'-\tfrac{1}{2}) \mp (l'+\tfrac{1}{2})]\cdot[(\zeta+\zeta')/(n+n') - \zeta']\cdot C^{m}_{l'\pm 1\,1\,l'}{}^{\mu m'}\cdot\langle nl'\pm 1m\zeta|n'l'm'\zeta\rangle \quad (11)$$

$$\langle n_A l_A m_A\zeta_A|\nabla_\mu|n_B l_B m_B\zeta_B\rangle = \zeta_B\cdot(4\pi/3)^{\frac{1}{2}}\Big(\sum_M C^{l_B+1\,1\,l_B}_{M\;\mu m_B}\cdot\{[(n_B-l_B-1)/\sqrt{n_B(n_B-\tfrac{1}{2})}]\langle n_A l_A m_A\zeta_A|n_B-1,l_B+1,M,\zeta_B\rangle - \langle n_A l_A m_A\zeta_A|n_B,l_B+1,M,\zeta_B\rangle\} + \sum_M C^{l_B-1\,1\,l_B}_{M\;\mu m_B}\cdot\{[(n_B+l_B)/\sqrt{n_B(n_B-\tfrac{1}{2})}]\langle n_A l_A m_A\zeta_A|n_B-1,l_B-1,M,\zeta_B\rangle - \langle n_A l_A m_A\zeta_A|n_B,l_B-1,M,\zeta_B\rangle\}\Big) \quad (12)$$

Table 2. Reduced one-electron matrix elements $\langle a\|u^f\|b\rangle$ of $[ML_3]^{2+}$

$\langle e\|u^{a_2}\|e\rangle = A$

		$\|e(e_g)\rangle$		$\|e(t_{2g})\rangle$		$\|e(\pi)\rangle$		$\|e(\pi^*)\rangle$	
		Ru	Fe	Ru	Fe	Ru	Fe	Ru	Fe
$\langle e(e_g)\|$	$\vec{r}$	0	0	0	0	0	0	0	0
	$\vec{r}\times\vec{\nabla}$	0	0	2	2	−0.0379	−0.0157	0.0335	0.0157
$\langle e(t_{2g})\|$	$\vec{r}$	0	0	0	0	0.0731	0.0291	0.0304	0.0127
	$\vec{r}\times\vec{\nabla}$	2.00	2.00	1.41	1.41	0.0267	0.0111	−0.0236	−0.001 11
$\langle e(\pi)\|$	$\vec{r}$	0	0	−0.0731	−0.0293	0	0	−0.779	−0.738
	$\vec{r}\times\vec{\nabla}$	0.0379	−0.0157	0.0267	0.0111	0.0300	0.0352	−0.833	−0.802
$\langle e(\pi^*)\|$	$\vec{r}$	0	0	−0.0304	−0.0127	0.779	0.738	0	0
	$\vec{r}\times\vec{\nabla}$	0.0335	0.0157	−0.0236	−0.0111	−0.833	−0.802	0.0264	0.0252

$\langle e\|u^e\|e\rangle = E$

		$\|e(e_g)\rangle$		$\|e(t_{2g})\rangle$		$\|e(\pi)\rangle$		$\|e(\pi^*)\rangle$	
		Ru	Fe	Ru	Fe	Ru	Fe	Ru	Fe
$\langle e(e_g)\|$	$\vec{r}$	0	0	0	0	0	0	0	0
	$\vec{r}\times\vec{\nabla}$	0	0	−2	−2	0.0378	0.0157	−0.0334	−0.0157
$\langle e(t_{2g})\|$	$\vec{r}$	0	0	0	0	0	0	−0.0210	−0.0134
	$\vec{r}\times\vec{\nabla}$	2	2	0	0	0	0	0	0
$\langle e(\pi)\|$	$\vec{r}$	0	0	0	0	−1.61	−1.55	0.348	0.364
	$\vec{r}\times\vec{\nabla}$	−0.0378	−0.0157	0	0	0	0	−0.810	−0.777
$\langle e(\pi^*)\|$	$\vec{r}$	0	0	−0.0210	−0.0134	0.384	0.364	−2.1	−2.06
	$\vec{r}\times\vec{\nabla}$	0.0334	0.0157	0	0	0.810	0.770	0	0

		$\langle e\|u^e\|a_2\rangle = C$		$\langle e\|u^e\|a_1\rangle = D$			
		$\|a_2(\pi^*)\rangle$		$\|a_1(t_{2g})\rangle$		$\|a_1(\pi)\rangle$	
		Ru	Fe	Ru	Fe	Ru	Fe
$\langle a_1(t_{2g})\|$	$\vec{r}$	0	0	0	0	0	0
	$\vec{r}\times\vec{\nabla}$	0	0	−2.0	−2.0	0.0757	0.0313
$\langle a_1(t_{2g})\|$	$\vec{r}$	0.009 46	−0.000 721	0	0	−0.0731	−0.0284
	$\vec{r}\times\vec{\nabla}$	0	0	−1.41	−1.41	0.0535	0.0222
$\langle a_1(t_{2g})\|$	$\vec{r}$	−0.392	−0.369	−0.0731	−0.293	1.64	1.71
	$\vec{r}\times\vec{\nabla}$	0.877	0.851	0.0267	0.0111	−0.0570	−0.0700
$\langle a_1(t_{2g})\|$	$\vec{r}$	−2.11	−2.06	0.0311	0.0127	−0.397	−0.379
	$\vec{r}\times\vec{\nabla}$	−0.005 37	−0.007 57	−0.0236	−0.0111	−0.834	−0.730

$\langle a_1\|u^{a_2}\|a_2\rangle = B$

		Ru	Fe
$\langle a_1(t_{2g})\|u^{a_2}\|a_2(\pi^*)\rangle$	$\vec{r}$	−0.0430	−0.0179
	$\vec{r}\times\vec{\nabla}$	0	0
$\langle a_1(\pi_g)\|u^{a_2}\|a_2(\pi^*)\rangle$	$\vec{r}$	0.577	0.529
	$\vec{r}\times\vec{\nabla}$	0.603	0.577

Table 3. State matrix elements†

$$\begin{aligned}
\langle a_1^2e^4,{}^1A_1|\vec{\nabla}|a_1^2e^3e^*,{}^1A_1\rangle &= (0,0,0)\\
\langle a_1^2e^4,{}^1A_1|\vec{\nabla}|a_1^2e^3e^*,{}^1A_2\rangle &= (0,0,\sqrt{2}A)\\
\langle a_1^2e^4,{}^1A_1|\vec{\nabla}|a_1^2e^3e^*,{}^1E\theta\rangle &= (0,E,0)\\
\langle a_1^2e^4,{}^1A_1|\vec{\nabla}|a_1^2e^3e^*,{}^1E\varepsilon\rangle &= (E,0,0)\\
\langle a_1^2e^4,{}^1A_1|\vec{\nabla}|a_1^2e^3a_2^*,{}^1E\theta\rangle &= (0,C,0)\\
\langle a_1^2e^4,{}^1A_1|\vec{\nabla}|a_1^2e^3a_2^*,{}^1E\varepsilon\rangle &= (C,0,0)\\
\langle a_1^2e^4,{}^1A_1|\vec{\nabla}|a_1{}^1e^4e^*,{}^1E\theta\rangle &= (0,-D,0)\\
\langle a_1^2e^4,{}^1A_1|\vec{\nabla}|a_1{}^1e^4e^*,{}^1E\varepsilon\rangle &= (-D,0,0)\\
\langle a_1^2e^4,{}^1A_1|\vec{\nabla}|a_1e^4a_2^*,{}^1A_2\rangle &= (0,0,B)
\end{aligned}$$

† For A,B,C,D reduced matrix elements, see Table 2.

State Transition Moments.—Using the computer program outlined in the previous section it is possible to calculate immediately the orbital transition moments within the basis of symmetry adapted functions given in Table 1. Single-zeta Slater type orbitals are used for the ligand atoms and double-zeta ones for the metal ions. The values of the screening parameters are taken from Clementi and Roeti [12] and the interatomic distances from *X*-ray data.[11] Note that a co-ordinate transformation from the system in Figure 2(*a*) to that in Figure 2(*b*) is necessary in order to have the C_3 axis coinciding with the *z* axis, which is the convention for trigonal symmetry. The 'orbital' matrix elements are transformed according to equation (4) into the reduced matrix elements, which are compiled in Table 2. From these values, it can be immediately seen which interactions lead to the largest dipole length moments and which to the largest magnetic moments.

The largest dipole length moments are the so-called 'transfer terms'. These are only found for planar transition moments (*e*) and are the contributions which were considered in earlier descriptions using a charge-transfer model.[5,13] They are followed in size by the π→π* transition moments, which are *ca.* 2—5 times smaller and have axial (a_2) and planar (*e*) polarization. All other dipole length matrix elements are more than two orders of magnitude smaller.

The largest reduced magnetic moment matrix elements are those connecting metal *d* orbitals. The next, about five times smaller, are the π→π* contributions. They are due to the three, helically arranged, localized π→π* transitions; another method of describing these contributions is the exciton theory.[14] Other

Table 4. Electrical and magnetic transition dipole moments of $[Ru(bipy)_3]^{2+}$ [a] and $[Fe(bipy)_3]^{2+}$ [a,b]

Transition	⟨ground state $\|\vec{r}\|$ excited state⟩	⟨ground state $\|\vec{r} \times \vec{\nabla}\|$ excited state⟩
$[Ru(bipy)_3]^{2+}$		
M.l.c.t.		
$A_2(a_1 \rightarrow a_2)$	$-0.0430 + 0.0575c$	$0.603c$
$A_2(e \rightarrow e)$	$0.0289 - 1.102d + 0.1034bd + 0.0430be$	$-0.0334 - 1.178d + 0.0373e + 2.0b$
$E(a_1 \rightarrow e)$	$0.0311 - 0.397c + 0.0731bc$	$0.0236 + 0.834c - 1.41b + 0.0535bc$
$E(e \rightarrow a_2)$	$0.0095 - 0.392d - 2.11e$	$0.877d - 0.00537e$
$E(e \rightarrow e)$	$-0.021 + 0.384d - 2.10e + 0.021be$	$-0.81d$
L.c.($\pi \rightarrow \pi^*$)		
$A_2(a_1 \rightarrow a_2)$	$0.557 + 0.0267f$	0.603
$A_2(e \rightarrow e)$	$-1.102 - 0.0288g + 0.1034b$	$-1.178 + 0.0334g - 0.0378b - 2.0bg$
$E(a_1 \rightarrow e)$	$-0.397 - 0.0311f + 0.0731b$	$0.834 - 0.0236f + 0.0535b + 1.41bf$
$E(e \rightarrow a_2)$	$-0.392 - 0.0095g$	0.877
$E(e \rightarrow e)$	$0.384 + 0.021g$	−0.81
M.c.($d \rightarrow d$)		
$E(a_1 \rightarrow e)$	$0.0311a - 0.397ac$	$2.0 + 0.0236a - 0.0757c + 0.834ac$
$E(e \rightarrow e)$	$0.021a + 0.384ac - 2.1ae$	$-2.0 - 0.0378a + 0.0334e - 0.81ac$
$A_2(e \rightarrow e)$	$0.0288a - 1.102ac$	$2.83 - 0.0334a - 0.536c + 0.474e - 1.178ac + 0.0373ae$
$[Fe(bipy)_3]^{2+}$		
M.l.c.t.		
$A_2(a_1 \rightarrow a_2)$	$-0.0179 + 0.135c$	$0.577c$
$A_2(e \rightarrow e)$	$0.018 - 1.044d + 0.0414bd + 0.018be$	$-0.0157 - 1.134d + 0.0356e + 2.0b - 0.0157bd + 0.0157be$
$E(a_1 \rightarrow e)$	$0.0127 - 0.379c + 0.0284bc$	$-0.0111 - 1.414b + 0.73c + 0.0222bc$
$E(e \rightarrow a_2)$	$-0.00072 - 0.369d - 2.06e$	$0.851d - 0.0757e$
$E(e \rightarrow e)$	$-0.0134 + 0.364d - 2.06e + 0.0134be$	$-0.77d$
L.c.($\pi \rightarrow \pi^*$)		
$A_2(a_1 \rightarrow a_2)$	$0.529 + 0.0179f$	0.577
$A_2(e \rightarrow e)$	$1.044 - 0.018g + 0.0414b$	$-1.134 + 0.001\,57g - 0.0157b - 2.0bg$
$E(a_1 \rightarrow e)$	$-0.379 - 0.0127 + 0.0284b$	$0.73 - 0.0111f + 0.0222b + 1.414bf$
$E(e \rightarrow a_2)$	$-0.369 + 0.000\,72g$	0.851
$E(e \rightarrow e)$	$0.364 + 0.0134g$	−0.770
M.c.($d \rightarrow d$)		
$E(a_1 \rightarrow e)$	$0.0127a - 0.397ac$	$2.0 + 0.0111a - 0.0313c + 0.73ac$
$E(e \rightarrow e)$	$-0.134a + 0.346ac - 2.06ae$	$-2.0 - 0.0157c + 0.0157e - 0.77ac$
$A_2(e \rightarrow e)$	$0.018a - 1.044ac$	$2.828 - 0.0157a - 0.222c + 0.222e - 1.134ac + 0.356ae$

[a] The coefficients a—g are defined in equation (5). [b] First-order perturbation: $b = e$, $d = c/2$, $c = g$, $d = f$.

reduced magnetic moments are considerably smaller. Transformation of these reduced orbital matrix elements to the m.o. basis given in equation (3) and further to state matrix elements using the relationships given in Table 3 is straightforward. The expressions of spin-allowed state matrix elements for the electric dipole length and the magnetic transition moments for the three m.c., five m.l.c.t., and five l.c. ($\pi \rightarrow \pi^*$) transitions are given in Table 4. These formulae can be used to calculate the relative intensities of the absorption and c.d. bands of these transitions for any set of mixing parameters a, b, and c.

Discussion

Comparison with the Experimental Spectra.—Comparison of the experimental spectra with the result of our calculations was made using a 'stick diagram'. The positions and intensities of the absorption and c.d. bands are compiled in Table 5 and compared with the experimental spectra in Figure 3(*a*) and (*b*). The positions of the lines are obtained by the following procedure. The trigonal splittings of the m.l.c.t., l.c. ($\pi \rightarrow \pi^*$), and m.c. bands are taken from the results of our earlier $MSX\alpha$ calculation.[10] Using this model, interelectronic repulsion is statistically averaged within a configuration. Therefore the states A_2 and E originating from the same orbital excitation are degenerated. More detailed calculations on the m.c. and m.l.c.t. excited states showed that one of these two states (E) is always lower in energy. The splitting is estimated to decrease with increased delocalization of the electrons, *i.e.* in the order m.c., m.l.c.t., l.c. states. The barycentres of the three groups of bands were estimated from the spectra; the m.l.c.t. and l.c. transitions are well localized. Of the m.c. transitions, only one is observed in the spectra of the $[FeL_3]^{2+}$ complex. This transition was tentatively assigned to a shoulder at the low-energy side of the m.l.c.t. transition [15] and to the additional peak at the low-energy end of the c.d. spectrum.[1,15] In case of $[RuL_3]^{2+}$ this transition is shifted to considerably higher energy due to the larger crystal-field splitting of second-row transition metal ions. Therefore the corresponding absorption band is not observed. It is buried under the strong m.l.c.t. and l.c. absorptions.

Qualitative inspection of Figure 3 shows that the correspondence between measured and calculated intensities is in general good within the group of m.l.c.t. and l.c. transitions. The rotational strength of the c.d. bands due to m.l.c.t. transitions is however too small compared to the l.c. transitions (note the factor of 10 in the stick diagram). The reason for this might be the abbreviation of the ligand π system, which surely has a considerable influence on the $\pi \rightarrow \pi^*$ transition moments and therefore disturbs them to a greater extent than the metal-centred ones. Such an imbalance will be shown mainly by the

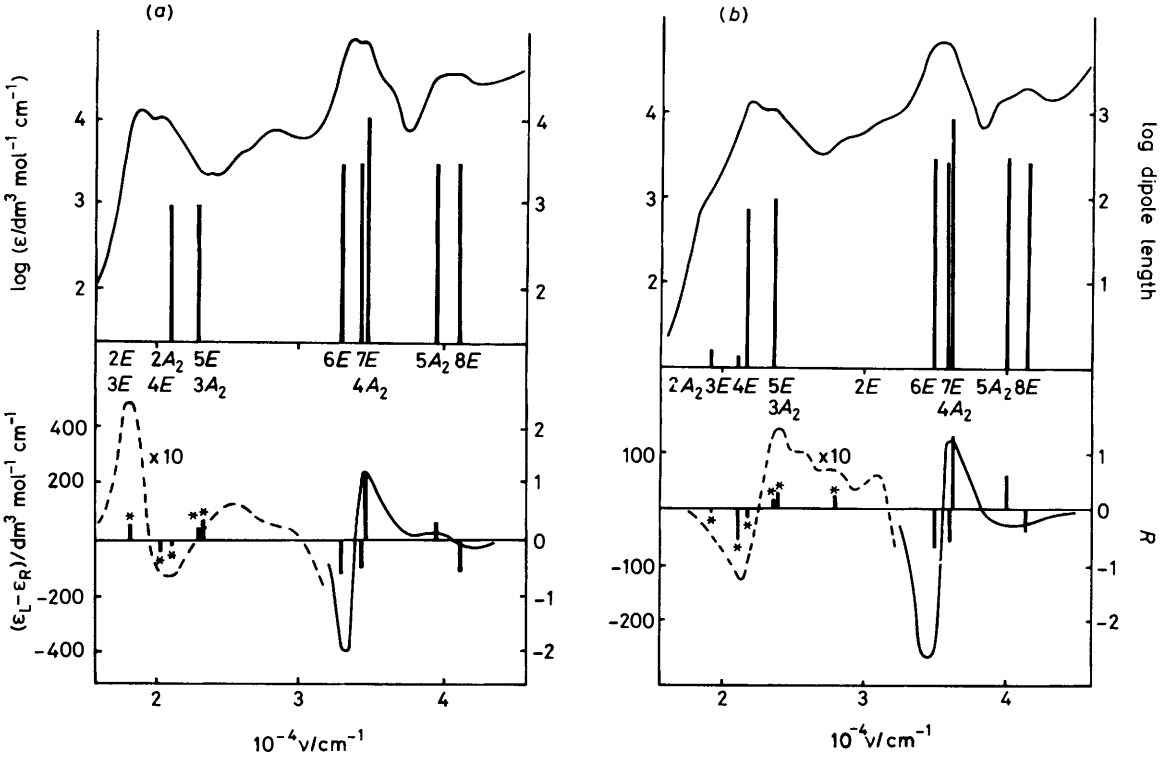

Figure 3 (*a*) Absorption and c.d. spectra of Δ-$[Fe(bipy)_3]^{2+}$ compared with the calculated stick diagram (• calculated rotational strength, 100). (*b*) Absorption and c.d. spectra of Δ-$[Ru(bipy)_3]^{2+}$ compared with the calculated stick diagram (• calculated rotational strength, 100)

Table 5. Band positions with calculated relative intensities (I) and rotational strengths (R) for $[FeL_3]^{2+}$ and $[RuL_3]^{2+}$ (L = NH=CH–CH=NH)

	$[FeL_3]^{2+}$	$10^{-3}E$/cm^{-1}	$I_{calc.}$	$R_{calc.}$
d–d	$E_1(a_1\rightarrow e)(1)$		1.37×10^{-9}	1.05×10^{-4}
	$E(e\rightarrow e)(2)$	18.0	8.39×10^{-7}	2.60×10^{-3}
	$A_2(e\rightarrow e)(1)$	18.0	5.09×10^{-10}	6.42×10^{-5}
M.l.c.t.	$A_2(a_1\rightarrow a_2)(2)$	18.4	2.74×10^{-4}	-9.55×10^{-5}
	$E(a_1\rightarrow e)(3)$	20.2	1.60×10^{-4}	-2.19×10^{-3}
	$E(e\rightarrow a_2)(4)$	20.9	8.70×10^{-2}	-1.25×10^{-3}
	$E(e\rightarrow e)(5)$	23.6	9.46×10^{-2}	1.67×10^{-3}
	$A_2(e\rightarrow e)(3)$	23.6	1.67×10^{-4}	2.35×10^{-3}
L.c.	$E(e\rightarrow a_2)(6)$	33	2.72×10^{-1}	-6.28×10^{-1}
π→π*	$E(e\rightarrow e)(7)$	34.6	2.65×10^{-1}	-5.61×10^{-1}
	$A_2(e\rightarrow e)(4)$	34.6	1.08	1.18
	$A_2(a_1\rightarrow a_2)(5)$	39.7	2.80×10^{-1}	-5.51×10^{-1}
	$E(a_1\rightarrow e)(8)$	41.1	2.83×10^{-1}	3.05×10^{-1}

	$[RuL_3]^{2+}$	$10^{-3}E$/cm^{-1}	$I_{calc.}$	$R_{calc.}$
d–d	$E(a_1\rightarrow e)(1)$		1.32×10^{-8}	3.25×10^{-4}
	$E(e\rightarrow e)(2)$	28.0	9.29×10^{-7}	2.72×10^{-3}
	$A_2(e\rightarrow e)(1)$	28.0	2.86×10^{-9}	1.53×10^{-4}
M.l.c.t.	$A_2(a_1\rightarrow a_2)(2)$	19.2	1.80×10^{-3}	-2.56×10^{-4}
	$E(a_1\rightarrow e)(3)$	21.0	1.48×10^{-3}	-5.93×10^{-3}
	$E(e\rightarrow a_2)(4)$	21.7	8.28×10^{-2}	-1.57×10^{-3}
	$E(e\rightarrow e)(5)$	23.8	1.05×10^{-1}	1.85×10^{-3}
	$A_2(e\rightarrow e)(3)$	23.8	5.67×10^{-4}	3.91×10^{-3}
π→π*	$E(e\rightarrow a_2)(6)$	34.5	3.07×10^{-1}	-6.88×10^{-1}
	$E(e\rightarrow e)(7)$	35.9	2.95×10^{-1}	-6.22×10^{-1}
	$A_2(e\rightarrow e)(4)$	35.9	1.19	1.29
	$A_2(a_1\rightarrow a_2)(5)$	40.0	3.10×10^{-1}	3.36×10^{-1}
	$E(a_1\rightarrow e)(8)$	41.4	3.06×10^{-1}	-6.57×10^{-1}

rotational strength of the m.l.c.t. transitions, which are composed of metal-centred magnetic moments and π→π* electric dipole moments (see below).

There are in a first-order perturbation model (Table 4) three adjustable mixing parameters (a, b, c) which determine the line intensities. We estimated these parameters as $a = 3 \times 10^{-3}$, $b = 1 \times 10^{-1}$, and $c = 1 \times 10^{-2}$ by trial and error to obtain a satisfactory agreement between calculation and experiment (Figure 3). In principle all parameters, the line positions and the mixing coefficients, could be determined by curve fitting if the experimental spectra were sufficiently well resolved to allow a unique deconvolution. The values of the adjustable parameters indicate that the mixing between the occupied t_{2_g} orbitals and the empty π* orbitals of the ligands given by b is dominant. This is in agreement with the previous work of Day and Sanders,[13] and more recently Ceulemans and Vanquickenborne,[5] who used a charge-transfer model to explain the absorption spectrum. This mixing can also be described as back-bonding, characterizing many of the chemical properties of these complexes. The mixing between the t_{2_g} and the occupied π orbitals has to be significantly smaller, as clearly indicated by the experiment. If this is not the case, π→π* 'borrowing' becomes the most important mechanism for the intensity of the m.l.c.t. bands. Under these conditions the axial and planar polarized absorptions would be of comparable intensity, in contrast to the experimental observations. The reason for the smaller t_{2_g}–π mixing must be due to a reduced overlap since the energy difference is comparable to the one between t_{2_g} and π*, as shown in Figure 1. The mixing between $e_g(d\sigma)$ and π* orbitals is very small. This is reasonable as this interaction is forbidden in O_h symmetry and mediated only by descent in symmetry.

The electric dipole moments of the m.c. *d–d* transitions are as expected very small. There is within our model only one transition to the $E(e\rightarrow e)$ which can efficiently borrow intensity from the transfer term and a $\pi\rightarrow\pi^*$ transition through the mixing between $e_g(d\sigma)$ and π^* orbitals. The magnetic dipole transition moments of all the three *d–d* transitions are large. This situation gives rise to one relatively intense c.d. band due to a *d–d* transition $E(e\text{–}e)(2)$. This band is clearly observed as an additional feature at low energy in the c.d. spectrum of $[Fe(bipy)_3]^{2+}$ (bipy = 2,2′-bipyridyl). The single-crystal c.d. spectrum[7] shows, that in accordance with our prediction, this band is polarized perpendicular to the three-fold axes. In $[Ru(bipy)_3]^{2+}$, where the ligand-field splitting is considerably larger, this band appears at higher energy. It is tentatively assigned to a shoulder between the m.l.c.t. and the l.c. transitions in the c.d. spectrum of $[Ru(bipy)_3]^{2+}$, which is absent in the spectrum of $[Fe(bipy)_3]^{3+}$. There are other mechanisms giving intensities to the forbidden *d–d* transitions such as vibronic coupling and *d–p* orbital mixing, which are not considered in our description. However, the fact that, in agreement with our model, only one of these transitions carries significant rotational strength, indicates that other contributions than the transfer term and $\pi\rightarrow\pi^*$ borrowing are of minor importance.

Of the five allowed m.l.c.t. transitions from the t_{2g} sub-shell to the π^* orbitals only two, $E(e\rightarrow a_2)(4)$ and $E(e\rightarrow e)(5)$, are predicted to carry considerable intensities. Both are polarized perpendicular to the three-fold axes (E). Hence it is reasonable to assign the two main features in the m.l.c.t. spectrum, the band at 21.55×10^3 cm^{-1} and the shoulder at 23.36×10^3 cm^{-1} for $[Ru(bipy)_3]^{2+}$ [16] and the bands at 18.62×10^3 cm^{-1} and 20.28×10^3 cm^{-1} for $[Fe(bipy)_3]^{2+}$ [17] to these transitions respectively. This result agrees with experimental observation. All the intense m.l.c.t. bands are perpendicularly polarized,[16,17] in agreement with the results obtained by Day and Sanders [13] and later by Ceulemans and Vanquickenborne,[5] applying charge-transfer (c.t.) theory. The dominant contribution to the electric dipole moment is of course the transfer term. The other three m.l.c.t. transitions gain intensity through $\pi\rightarrow\pi^*$ borrowing or the so-called 'contact term'. These mechanisms are in general not included in the c.t. model.

No detailed information can therefore be obtained about the intensities of the above bands within the c.t. model. Our calculation shows that these borrowing mechanisms are considerably less effective than the transfer term. Hence the electric dipole moments are *ca.* 10 times smaller and their absorption intensity is about two orders of magnitude smaller (note the logarithmic scale in Figure 3). The magnetic dipole moments are dominated by the *d–d* contributions. Again, only two of the m.l.c.t. transitions, $A_2(e\rightarrow e)$ and $E(a_1\rightarrow e)$, can couple with the *d–d* transition moments. The other three transitions borrow magnetic moments from the $\pi\rightarrow\pi^*$ transition. This is less effective and their magnetic transition moments are *ca.* 10^2 times smaller. We can therefore distinguish three types of m.l.c.t. transitions: (*i*) the two mentioned above, $E_1(e\rightarrow a_2)(4)$ and $E_2(e\rightarrow e)(5)$, with a large electric dipole moment and hence with strong absorption, and having a small magnetic dipole moment; (*ii*) the $A_2(e\rightarrow e)(3)$ and $E(a_1\rightarrow e)(3)$ transitions, with a large magnetic and a small electric dipole moment, hence showing strong c.d. bands; (*iii*) one $A_2(a_1\rightarrow a_2)(2)$ transition which carries neither a large electric nor a large magnetic dipole moment. This result is in agreement with the conclusion of Ferguson *et al.*[7] drawn from their single-crystal c.d. spectra, stating that the intense bands which are observed in the absorption and c.d. spectra are due to different transitions.

There are five $\pi\rightarrow\pi^*$ transitions, which carry all comparable intensities in the absorption spectrum and in the c.d. spectrum. The sign of the rotational strength is positive for those polarized parallel to the C_3 axes (a_2) and negative for those perpendicular (e) in the case of complexes with the absolute configuration Δ. This is in agreement with the predictions made by exciton theory [14] based on three independent chromophores. The two transitions of lowest energy correspond to orbital excitations $e\rightarrow a_2$ and $e\rightarrow e$. These two excitations are considered in exciton theory as the origin for a characteristic doublet with different signs, which allow determination of the absolute configuration of the complexes.[14] Our calculation shows that, in the $e\rightarrow e$ excitation, which gives rise to two transitions $A_2(e\rightarrow e)(4)$ and $E(e\rightarrow e)(7)$, the $A_2(e\rightarrow e)(4)$ component has dominant rotational strength. Therefore, the two observed bands of lowest intensity in the $\pi\rightarrow\pi^*$ region are polarized perpendicular and parallel in order of increasing energy, which leads to the characteristic (−),(+) doublet observed in the $\pi\rightarrow\pi^*$ region of the c.d. spectrum of the Δ-$[ML_3]^{2+}$ complexes.

Appendix

Invariance of the Rotational Strength with Respect to Co-ordinate Transformation.—Since we use dipole lengths rather than dipole velocities in equation (2) we have to show that the rotational strength is origin-independent. Suppose the co-ordinate transformation between the system (x,y,z) and (x',y',z') is defined as in equation (A1), where $\vec{r}$ and $\vec{r}'$ are vectors in

$$\vec{r} = M\vec{r}' + \vec{r}_0 \qquad \text{(A1)}$$

(x,y,z) and (x',y',z') respectively; $\vec{r}_0$ is the vector representing the translation of origin, and M is a unitary matrix. Then the scalar product $\langle A|\vec{r}|B\rangle\ \langle B|\vec{r}\times\vec{\nabla}|A\rangle$, which determines the rotational strength, is transformed as in equation (A2). Since

$$\langle A|M\vec{r}'|B\rangle = \langle B|(M\vec{r}')\times(M\vec{\nabla}')|A\rangle + \langle A|M\vec{r}'|B\rangle(\vec{r}_0'\times\langle B|M\nabla'|A\rangle) \qquad \text{(A2)}$$

unitary transformations leave the scalar product invariant, the first and second terms of equation (14) are, respectively, written as in expressions (A3) and (A4) where $\vec{r}_0 = M^\dagger\vec{r}_0'$, $M^\dagger$ being the

$$\langle A|\vec{r}'|B\rangle\cdot\langle B|\vec{r}'\times\vec{\nabla}'|A\rangle \qquad \text{(A3)}$$

$$\langle A|\vec{r}'|B\rangle\cdot(\vec{r}_0\times\langle B|\vec{\nabla}'|A) \qquad \text{(A4)}$$

conjugate matrix of M. The second term is a so-called 'mixed product' measuring the volume of the parallelepiped spanned by the three vectors $\langle A|\vec{r}|B\rangle$, $\vec{r}_0$, and $\langle B|\vec{\nabla}'|A\rangle$. This term vanishes if any of the three vectors are collinear. If $\langle A|$ and $|B\rangle$ are Eigenfunctions of the Hamiltonian, $\langle A|\vec{\nabla}|B\rangle = -\frac{m}{h^2}\varepsilon\langle A|\vec{r}|B\rangle$ where m/h^2 is a constant and ε is the transition energy. However, for approximate wavefunctions (as those employed here) this equation does not generally hold. Nevertheless, in the present case, in which molecules have D_3 symmetry, it can be proven to vanish by symmetry considerations. Clearly the matrix elements of $\vec{\nabla}$ and $\vec{r}$ connecting the ground state of symmetry A_1 with any of the excited states are of the form given below. Thus $\langle A|\vec{r}|B\rangle$ and $\langle B|\vec{\nabla}|A\rangle$ are parallel also for approximate wavefunctions, provided they are bases of

$\langle A_1\|\vec{\nabla}\|A_1\rangle = (0,0,0)$	$\langle A_1\|\vec{r}\|A_1\rangle = (0,0,0)$
$\langle A_1\|\vec{\nabla}\|A_2\rangle = (0,0,\ldots)$	$\langle A_1\|\vec{r}\|A_2\rangle = (0,0,\ldots)$
$\langle A_1\|\vec{\nabla}\|E\theta\rangle = (0,\ldots,0)$	$\langle A_1\|\vec{r}\|E\theta\rangle = (0,\ldots,0)$
$\langle A_1\|\vec{\nabla}\|E\varepsilon\rangle = (\ldots,0,0)$	$\langle A_1\|\vec{r}\|E\varepsilon\rangle = (\ldots,0,0)$

irreducible representations. Hence the second term, equation (A4), vanishes for any $\vec{r}_0$ and the rotational strength can be said to be invariant under any co-ordinate transformation.

Acknowledgements

This work was supported by the Swiss National Science Foundation.

References

1 A. J. McCaffery, S. F. Mason, and B. J. Norman, *J. Chem. Soc. A*, 1969, 1428.
2 I. Hanazaki and S. Nagakura, *Inorg. Chem.*, 1969, **8**, 648.
3 J. Blomquist, B. Norden, and B. Sundbom, *Theor. Chim. Acta*, 1973, **28**, 313.
4 B. Mayoh and P. Day, *Theor. Chim. Acta*, 1978, **49**, 259.
5 A. Ceulemans and L. G. Vanquickenborne, *J. Am. Chem. Soc.*, 1981, **103**, 2238.
6 S. F. Mason, *Inorg. Chim. Acta*, 1968, 89.
7 J. Ferguson, F. Herren, and G. M. McLauglin, *Chem. Phys. Lett.*, 1982, **89**, 376.
8 N. Sanders and P. Day, *J. Chem. Soc. A*, 1970, 1190.
9 J. S. Griffith, 'The irreducible tensor method for molecular symmetry groups,' Prentice Hall, Englewood Cliffs, New Jersey, 1962.
10 C. Daul and J. Weber, *Chem. Phys. Lett.*, 1981, **77**, 593.
11 D. P. Rillema, D. S. Jones, and H. A. Levy, *J. Chem. Soc., Chem. Commun.*, 1979, 849.
12 E. Clementi and C. Roeti, *At. Data Nucl. Data Tables*, 1974, **14**, 177.
13 P. Day and N. J. Sanders, *J. Chem. Soc. A*, 1967, 1536.
14 B. Bosnich, *Inorg. Chem.*, 1968, **7**, 2379.
15 J. Ferguson and F. Herren, *Chem. Phys.*, 1983, **76**, 45.
16 F. Felix, J. Ferguson, H. U. Guedel, and A. Ludi, *J. Am. Chem. Soc.*, 1980, **102**, 4096.
17 S. Decurtins, F. Felix, J. Ferguson, H. U. Guedel, and A. Ludi, *J. Am. Chem. Soc.*, 1980, **102**, 4102.

Received 3rd *December* 1986; *Paper* 6/2335